Pergamon

Int. J. Heat Mass Transfer. Vol. 40, No. 17, pp. 4169–4181, 1997

Printed in Great Britain
0017–9310/97 $17.00+0.00

PII: S0017–9310(97)00027–6

Estimation of thermal conductivity of thermoplastics under moulding conditions: an apparatus and an inverse algorithm

T. JURKOWSKI, Y. JARNY and D. DELAUNAY
Laboratoire de Thermocinétique, ISITEM, BP 90604, 44306 Nantes Cedex 03, France

(*Received* 22 *December* 1995 *and in final form* 12 *December* 1996)

Abstract—The thermal conductivity of thermoplastics is measured under moulding conditions (high pressure and high temperature). A specific apparatus has been designed and is described. A parameter estimation method is used for the experimental data processing. It is based on the resolution of a 1-D non-linear inverse conduction problem. The optimisation algorithm developed to solve the problem, is efficient and stable. Confidence intervals of the estimated parameters take into account errors both in the temperature measurements and in the parameters of the model. Heat capacity is estimated from calorimetric measurements, error analysis on the estimated conductivity is discussed, especially in the phase change interval. Numerical validation and experimental examples are presented. © 1997 Elsevier Science Ltd.

INTRODUCTION

Heat transfer analysis in moulding processes of thermoplastic materials are usually performed today by using industrial software. Accurate data of these thermal properties are thus required. The lack of knowledge in this domain was a motivation for this work. We describe an experimental apparatus and a numerical method, which enable the determination of thermal conductivity of thermoplastics over a wide range of temperature, involving a phase change. The apparatus has been studied to deal with the conditions of polymer injection in a mould: pressure up to 80 MPa and temperature up to 400°C. In the temperature range considered, the thermophysical properties of materials are varying with temperature. Classical methods (hot guarded plate, radial flux, line source method, flash method) are not well adapted to estimate thermal conductivity in such conditions (high pressure and temperature) and to deal with the non-linear heat transfer equations, especially in the phase change region. The method which is presented is based on the inverse analysis of non linear transient heat conduction as in [1], but here temperature measurements are recorded at the boundary of a thin sample.

The first part of this paper is devoted to the inverse parameter estimation method and to its numerical implementation. Some peculiarities of the method are underlined: thermal contact resistance (TCR) resulting from the external location of the sensors is considered in the model, convergence of the iterative optimisation algorithm is improved, evaluation of errors on the estimated parameters due to measurement errors and model errors is studied. Validation of the method is based on numerical experiments which reproduce solidification of a semicrystalline thermoplastic. In the second part, a description of the apparatus is given, and the main choices of its design are discussed. In the last part, data processing of experimental measurements, recorded during solidification of two polymers, are presented.

ESTIMATION PROBLEM

The estimation method is based on the comparison between measured and calculated temperatures during the cooling of the polymer. The configuration scheme and the modelling equations are described in order to formulate the estimation problem.

Configuration scheme

The apparatus can be schematised by a multilayer symmetrical configuration [2], it includes a central plate, two investigated samples and two heat exchangers (Fig. 1). Heat transfer is supposed to be unidirectional in the axiswise and symmetrical relative to the central plate. Due to this symmetry, the heat transfer analysis can be limited to one sample only. The temperature distribution in the thickness of the central plate is considered uniform because of the high value of the metallic thermal diffusivity compared to the polymer diffusivity, the ratio is about 100. Heat flux density $\varphi_0(t)$ transferred between the central plate and the sample during the solidification can be then easily obtained in this symmetrical configuration from the temperature measurement $T_0(t)$ of the central plate, $\varphi_0(t)$ satisfies the enthalpy balance equation:

$$\varphi_0(t) = \frac{1}{2} b_p \rho_p c_p \frac{dT_0}{dt}(t) \quad (1)$$

NOMENCLATURE

J	residual criterion to be minimised	η	vector of calculated temperature
J_W	modified residual criterion	φ	heat fluid density
L	thickness of the sample	λ	thermal conductivity
R	thermal contact resistance	θ	temperature
t	time	σ	standard deviation.
X	sensitivity matrix		
Y	vector of measured temperature.	Subscripts and superscripts	
		i	space discretisation index
Greek symbols		j	parameter index
β	vector of estimated parameters	k	iteration number
ε	descent depth	n	time index.

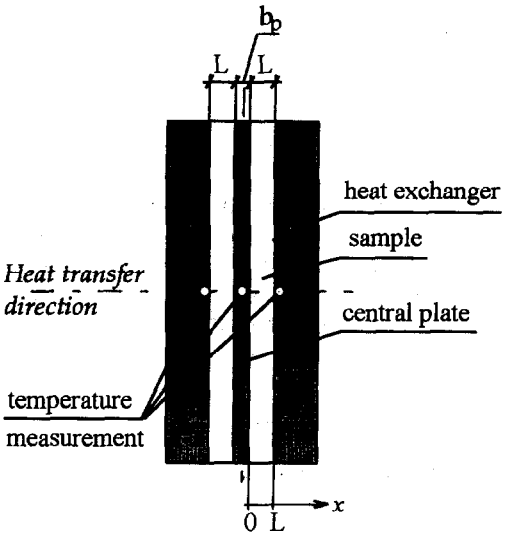

Fig. 1. Experimental configuration.

b_p is the thickness of the central plate, ρ_p its mass density and c_p its specific heat.

Model equations

The temperature $\theta(x, t)$ in the sample, for $t \in [0, t_f]$, is the solution of the non-linear heat conduction equations:

$$C(\theta)\frac{\partial\theta}{\partial t}(x,t) - \frac{\partial}{\partial x}\left[\lambda(\theta)\frac{\partial\theta}{\partial x}\right] = 0 \quad 0 < x < L \tag{2a}$$

$$-\lambda(\theta)\frac{\partial\theta}{\partial x}(0,t) = \varphi_0(t) \quad x = 0 \tag{2b}$$

$$R_L(t)\left[\lambda(\theta)\frac{\partial\theta}{\partial x}(L,t)\right] + \theta(L,t) = T_L(t) \quad x = L \tag{2c}$$

$$\theta(x,0) = T^0(x) \quad \text{(initial condition)} \tag{2d}$$

φ_0 is the heat flux density at $x = 0$, estimated from equation (1), T_L is the measured temperature at the surface of the heat exchanger, R_L the thermal contact resistance at this interface.

At the boundary $x = 0$, a thermal contact resistance R_0 is also considered, then the calculated temperature of the central plate $\theta_0(t)$ and the temperature of the sample at the interface $\theta(0, t)$ are linked by the measurement equation:

$$\theta_0(t) = \theta(0,t) + R_0(t)\varphi_0(t) \tag{3}$$

θ_0 is called the model response.

Numerical approximation

The space variable is discretised with finite differences, Fig. 2, and a Crank–Nicolson scheme is used to discretise the time variable. The thermal conductivity λ and the volumetric heat capacity $C(=\rho \times c_p)$ are assumed to be variable with temperature. A temperature table θ_j $(j = 1, \ldots, m)$, is given, then variation of $\lambda(\theta)$ are described by piecewise linear functions ω_j and defined by the values (λ_j, θ_j), $j = 1, \ldots, m$, where m is the number of the basic function ω_j

$$\lambda(\theta) = \sum_j^m \lambda_j \omega_j(\theta). \tag{4}$$

The piece-wise functions ω_j are described in Table 1.

The temperature field $\theta(x_i, t^n)$ in the polymer is approximated at time t_n by the vector $U^n = [U_i^n, i = 0, 1, \ldots, N]$, $n = 1, \ldots, NT$. U^n is solution of

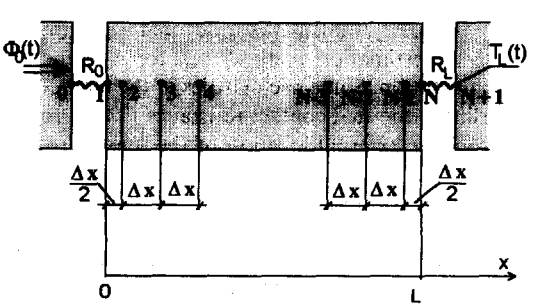

Fig. 2. Space discretisation.

Table 1. The piece-wise linear functions ω_j

	$\theta\in]-\infty,\theta_{j-1}[$	$\theta\in[\theta_{j-1},\theta_j]$	$\theta\in]\theta_j,\theta_{j+1}]$	$\theta\in]\theta_{j+1},+\infty[$
$j=1$		1	$\omega_j(\theta)=\dfrac{\theta_{j+1}-\theta}{\theta_{j+1}-\theta_j}$	0
$j=2,\ldots,m-1$	0	$\omega_j(\theta)=\dfrac{\theta-\theta_{j-1}}{\theta_j-\theta_{j-1}}$	$\omega_j(\theta)=\dfrac{\theta_{j+1}-\theta}{\theta_{j+1}-\theta_j}$	0
$j=m$	0	$\omega_j(\theta)=\dfrac{\theta-\theta_{j-1}}{\theta_j-\theta_{j-1}}$		1

a non-linear matrix equation which is the discretised form of equations (2) and (3):

$$[G]U^{n+1}=[H]U^n+V. \tag{5}$$

The tridiagonal matrices $[G]$, $[H]$ and the vector V are given in the appendix (Table 5).

Formulation of the estimation problem

In the following, the standard notations used in parameter estimation [3] are adopted:

- the parameter vector β to be determined, is related to the unknown function $\lambda(\theta)$ by:

$$\beta=[\lambda_1,\ldots,\lambda_m]\in\mathbf{R}^m$$

- the observation vector Y (dimension $NT\times 1$) corresponds to the measured temperature $T_0(t_n)$ given by the sensor in the central plate, at the discrete times t_n, $n=1,\ldots,NT$;
- the response vector $\eta(\beta)$ (dimension $NT\times 1$), corresponds to the calculated temperature $\theta_0(t_n)$ given by the heat transfer modelling equations (2) and (3). The model response of the discretised equations (5) is $\eta^n(\beta)=U_0^n$;
- the difference $Y-\eta(\beta)$ and $J(\beta)=(1/2)[Y-\eta(\beta)]^{\mathrm{T}}[Y-\eta(\beta)]$ are called, respectively, the residual vector and the residual criterion, hence the gradient of $J(\beta)$ is:

$$\nabla J(\beta)=-X^{\mathrm{T}}(\beta)[Y-\eta(\beta)]. \tag{6}$$

The matrix $X(\beta)$, called sensitivity matrix, is defined by:

$$X_{nj}(\beta)=\frac{\partial\eta^n(\beta)}{\partial\beta_j}\quad n=1,\ldots,NT, j=1,\ldots,m. \tag{7}$$

The estimation problem considered in this paper consists in determining $\beta^*\in\mathbf{R}^m$ which minimises the modified residual criterion J_{W}:

$$J_{\mathrm{W}}(\beta)=\tfrac{1}{2}[Y-\eta(\beta)]^{\mathrm{T}}[Y-\eta(\beta)]+\tfrac{1}{2}[\mu-\beta]^{\mathrm{T}}W[\mu-\beta] \tag{8}$$

where μ is a known vector $(m\times 1)$, and W a known matrix $(m\times m)$. The choices of μ and W depend on the optimisation algorithm and the effect of the term $[\mu-\beta]^{\mathrm{T}}W[\mu-\beta]$ on the estimation procedure will be discussed in the next section. The main idea is to improve stability, that is to reduce fluctuations in the iterative determination of the parameters and to ensure fast convergence of the procedure.

Sensitivity matrix

According to equation (6), the X matrix is needed for the computation of the gradient of the criterion $\nabla J(\beta)$. Its elements, defined by equation (7), are first computed from the set of equation (9), which comes from the derivation of equation (5); (one equation for each component β_j):

$$[G](U^{n+1})'_j=[H](U^n)'_j-[G]'U^{n+1}+[H]'U^n+V'_j \tag{9}$$

where $(U^n)'_j$ is the derivative of the vector U^n with respect to the parameter β_j, at time t_n. Matrices $[G]$ and $[H]$ are the same as in the direct problem and $[G]'_j[H]'_j$, V'_j are the derivatives of $[G]$, $[H]$ and V. Equations (9) are linear. They are solved for j varying from 1 to m. Finally, we obtain the elements of X by:

$$X_{nj}=\frac{\partial\eta^n}{\partial\beta_j}=(U_0^n)'_j\quad n=1,\ldots,NT;\ j=1,\ldots,m. \tag{10}$$

ESTIMATION METHOD

The iterative algorithm

The minimisation problem is solved iteratively. By taking $\mu=\beta^{(k)}$ in equation (8) the minimisation is achieved according to the following general recurrent formula (k = iteration number), Beck[4]:

$$\beta^{(k+1)}=\beta^{(k)}-\varepsilon^{(k+1)}[P(\beta^{(k)})]^{-1}\nabla J(\beta^{(k)}) \tag{11a}$$

with

$$P(\beta^{(k)})=X^{\mathrm{T}}(\beta^{(k)})X(\beta^{(k)})+W^{(k+1)}. \tag{11b}$$

The stability and the rapidity of iterative procedure depends on the choice of $W^{(k)}$ and the positive scalar $\varepsilon^{(k)}$, named "descent depth". Let us describe our choice of these parameters, in order to compare the resulting algorithm with the standard Gauss, Levenberg and Marquardt methods.

In the Gauss method, [5, 3], the matrix $W^{(k)}$ is equal

to zero, $\varepsilon^{(k)}$ is equal to one, and the iterative formula (11a, 11b) is reduced to:

$$\beta^{(k+1)} = \beta^{(k)} + [X^{\mathrm{T}}(\beta^{(k)})X(\beta^{(k)})]^{-1}[X^{\mathrm{T}}(\beta^{(k)})[Y-\eta(\beta^{(k)})]]. \quad (12)$$

In the Levenberg and Marquardt methods, the matrix W is diagonal, $\varepsilon^{(k)}$ is equal to one, the second term of $J_{\mathrm{W}}(\beta)$ is taken in the form:

$$[\beta^{(k)}-\beta^{(k+1)}]^{\mathrm{T}}W^{(k+1)}[\beta^{(k)}-\beta^{(k+1)}]. \quad (13)$$

In the Levenberg method [6], a constant matrix W is taken to avoid the oscillations of $\beta^{(k)}$ during iterations, but the choice of W is delicate: low values of W will give no influence for limiting the instability of parameters $\beta^{(k)}$, high values will reduce extremely the convergence rapidity (see comparisons of Davies *et al.* [7]). It is interesting to notice that even near to the minimum, where this second term of the criterion (8) becomes very small (10^{-4}–10^{-6} compared to the first iterations), convergence of the Levenberg method remains very slow. It can be explained by the fact, that even if the second term of the criterion vanishes, equation (13), the W terms which modify the matrix P remain unchanged.

In the Marquardt algorithm [8], the matrix $W^{(k)}$ is changed at each iteration. In fact, the iterative process of minimisation, equation (11a, b), can be expressed in the general form:

$$\beta^{(k+1)} = \beta^{(k)} + \varepsilon^{(k+1)}\Delta\beta^{(k)} \quad (14)$$

$$\Delta\beta^{(k)} = -[P^{(k)}]^{-1}\nabla J^{(k)} \quad (15)$$

where $\Delta\beta^{(k)}$ is the descent direction. It can be noted that if the matrix P is diagonal and if its elements have the same order of magnitude, the direction $\Delta\beta$ becomes closer to the direction ∇J. Hence, modification of the P diagonal elements will change the descent direction, and consequently the convergence of the procedure. It can be proved that by acting on the P diagonal elements, one can always ensure convergence of the optimisation procedure [9]. To facilitate the operations on P, Marquardt proposed to normalise the terms of equation (15), according to the formulas (16). Moreover, the normalisation of the P improves the computation of the inverse P^{-1}:

$$p_{ij}^{*} = \frac{p_{ij}}{\sqrt{p_{ii}}\sqrt{p_{jj}}} \qquad \nabla J_j^{*} = \frac{\nabla J_j}{\sqrt{p_{jj}}}$$

and finally

$$\Delta\beta_j = \frac{\Delta\beta_j^{*}}{\sqrt{p_{jj}}}. \quad (16)$$

The idea of the Marquardt method consists in looking for an optimal descent direction, at each iteration. A positive term c added to the diagonal terms of the normalised matrix P^{*} adjusts this direction. For two different values of c, two $\Delta\beta$ are obtained, the corresponding criteria are compared and better direction is chosen. If there is no convergence (the criterion does not diminish), the value of c will be increased, until the criterion decreases. In practice, this procedure leads to double (at least) the number of resolutions of the direct problem at each iteration, and increases considerably the total number of iterations [7].

The method we developed [10], consists in taking the advantages of these algorithms: rapidity (Gauss), stability (Levenberg) and convergence (Marquardt), and in avoiding: low convergence (Levenberg, Marquardt), time consuming computation (Marquardt), difficulty to find the appropriate value of the "governor" coefficient (Levenberg), and divergence (Gauss, for the multi-parametric and highly non-linear problems).

One can notice that the choice of the matrix W is not very restrictive, the main constraint is to ensure convergence to the minimum. It can be observed that by setting $\mu = \beta^{(k)}$ in equation (8):

(1) only the diagonal of $P^{(k)}$ will be modified in the iterative expression, equation (11), compared to Gauss method ($W = 0$). The term $\nabla J = -X^{\mathrm{T}}(Y-\eta)$ remains unchanged.

(2) during the final iterations, $\beta^{(k+1)}$ is close to $\beta^{(k)}$, the second part of the criterion J_{W} vanishes, so there will be no bias between minima β^{*} found with the modified criterion $J_{\mathrm{W}}(W \neq 0)$ and with a nonmodified criterion $J(W = 0)$.

So our choice of the regulating diagonal matrix $W^{(k)}$ is:

$$w_{jj}^{(k)} = \delta\frac{\nabla J_j^{(k)}}{(\nabla J_j)^{k=0}}x_{jj}^{2(k)} \quad (17)$$

where δ = real number between 10^{-3} and 10^{+3} (for unstable problems the higher value is taken); $\nabla J_j^{(k)}$ = gradient component of the residual criterion, iteration k; $(\nabla J_j)^{k=0}$ = same component, for initial iteration; $x_{jj}^{2(k)}$ = diagonal term of the matrix $X^{\mathrm{T}}X$ (if $X^{\mathrm{T}}X$ is normalised, $x_{jj}^{2} = 1$), iteration k.

This procedure has the following advantages: for high values of the gradient, the descent direction will approach to the gradient direction, and for moderate slopes (near to the minimum) this direction is similar to this of Gauss method. Consequently, the stabilisation of the procedure is ensured far from the minimum, precision and rapidity near to the minimum. During final iterations, the ratio $\nabla J_j^{(k)}/\nabla J_j^{(0)}$ goes to zero and P becomes close to $X^{\mathrm{T}}X$. This property allows to choose δ large enough to get stability in the first iterations, without risk of slowing down the next steps, as in the case of the Levenberg method. We recommend the value $\varepsilon \approx 0.6$–0.8, instead of $\varepsilon = 1$, in order to avoid oscillations.

Error analysis

In order to estimate the accuracy of the results, confidence intervals of the identified parameters have

to be determined. There are mainly two kinds of errors: errors which are superimposed on measured quantity (on temperature, in our case), and model errors due to the uncertainty on some parameters (sample thickness, heat capacity or others). The second kind of error gives bias on the model response $\eta(\beta)$.

Measurement errors are usually assumed to be gaussian, zero mean, with constant variance σ^2. For instance, it could be a noise from the data acquisition circuit (measuring apparatus, amplifiers, etc.), added to the exact signal. The error analysis [11, 12] of this kind of noise, leads to the standard deviation of the estimated parameters β:

$$\sigma_\beta = \sigma[\mathrm{diag}(X^{\mathrm{T}}X)^{-1}]^{1/2}. \tag{18}$$

Confidence intervals are then easily determined. According to statistical rules, for example, the probability to have the parameter in the interval $[\beta_j \pm 2.58\sigma_{\beta j}]$ is 99%. This approach is used by many authors. Hence, confidence intervals are generally very "tight", estimated errors are often less than 1% and practically always unrealistic. Nevertheless, this evaluation does not take into account the main source of error: the inexactitude of model parameter values, which usually come from other measurements. Thus, a bias $\delta\eta$ is introduced into the calculated temperature. That kind of error is very frequent in practice: sample thickness, sensor location, thermophysical parameters are always known with some uncertainty.

Hence, the interest to evaluate the error on the estimated parameter vector values β, resulting from these modelling errors is evident. In our case, four model parameters have been considered: volumetric heat capacity of the sample, heat flux density on the boundary, thermal contact resistance and sample thickness. To deal with that question, we have adopted the following procedure based on the sensitivity equation [13].

Step no. 1. For each parameter p of the model, an interval $[p_1, p_2]$ is considered. Let $p_{ex} \in [p_1, p_2]$ be the exact value, a bias coefficient b and the corresponding variation δb are introduced:

$$p = b \times p_{ex} = p_{ex} \times (1 + \delta b) \quad p_1 \leqslant p \leqslant p_2.$$

Then for $p = p_1$ and $p = p_2$, the extreme variations $\delta b_1 \leqslant 0$ and $\delta b_2 \geqslant 0$ are determined.

Step no. 2. For δb sufficiently small, the resulting bias $\delta\eta$ on the calculated temperature is:

$$\delta\eta = \frac{\partial\eta}{\partial b}\delta b = X(b)\delta b \tag{19}$$

and according to equation (10), the corresponding variation $\delta\beta$ of the parameter β, due to the bias temperature $\delta\eta$ is:

$$\delta\beta = P^{-1}X^{\mathrm{T}}(\beta)\delta\eta \tag{20}$$

hence

$$\delta\beta = P^{-1}X^{\mathrm{T}}(\beta)X(b)\delta b = \frac{\partial\beta}{\partial b}\delta b. \tag{21}$$

The matrix $[P^{-1}]$ and $[X(\beta)]$ are already computed in the iterative process (equations (9), (10), (17)). The vector $X(b)$ is calculated by taking the derivative of the discrete equations (5), in the same way that for $X(\beta)$. For each bias coefficient b, a linear sensitivity equation has to be solved. Solution $(U)'_b$ calculated at the sensor location abscissa $x = 0$ gives $X(b)$:

$$[G](U^{n+1})'_b = [H](U^n)'_b - [G]'_b(U^{n+1}) + [H]'_b(U^n) + V'_b. \tag{22}$$

Only derivatives of the matrices G, H and vector V are needed. Each parameter p belongs to each element of these two matrices or vector. Each of their elements, denoted by a_{ij}, takes one of the two following forms:

(1) $a_{ij} = A_{ij}p^2$ (case of thickness)

or

(2) $a_{ij} = A_{ij}p$ (other parameters)

where A_{ij} is a scalar independent of p and can be equal to zero. Derivatives of a_{ij} with respect to the bias coefficient b are, respectively for case 1 and case 2:

$$(1) \quad \frac{\partial a_{ij}}{\partial b} = (A_{ij}p^2)' = (A_{ij}b^2p_{ex}^2)' = 2A_{ij}bp_{ex}^2 = 2A_{ij}b\frac{p^2}{b^2} = \frac{2}{b}a_{ij}$$

$$(2) \quad \frac{\partial a_{ij}}{\partial b} = (A_{ij}p)' = (A_{ij}bp_{ex})' = A_{ij}p_{ex} = A_{ij}\frac{p}{b} = \frac{1}{b}a_{ij}.$$

Hence, computation of the matrix derivatives $[G]'_b$, $[H]'_b$, V'_b, equation (22), is evident.

Step no. 3. The extreme variations $\delta\beta_1$ and $\delta\beta_2$ are then computed with the values of δb_1 and δb_2, following equation (21), and the lower and upper bounds of errors $\delta\beta$ are summed. For errors less than $\partial\beta/\beta < 10\%$, this assumption of additive errors is fairly correct. For more important errors, a good approximation of the confidence intervals is, thus, obtained and the procedure gives information on systematic errors in the residual measurement.

Following this above analysis, the effect of a possible asymmetrical configuration on the estimated parameter β has also been studied. It was verified that the chosen configuration is not very sensitive to that kind of error [2]. For example, 5% of difference in the sample thicknesses causes a parameter identification error less than 1%.

RESULT ANALYSIS

Numerical validation of the method

To validate the method and to compare results with several classical algorithms, a numerical example which simulates the solidification of a semicrystalline

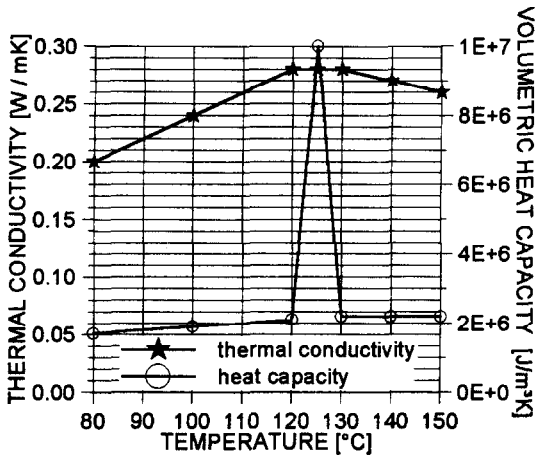

Fig. 3. Thermal parameters of the material.

thermoplastic is chosen. The solution of the direct problem is computed with the following data. Sample thickness is $L = 0.004m$, total experiment time $t_f = 200$ s. The temperature goes from $T^0 = 150$–80°C. Phase change occurs in the range [120°C, 130°C]. Phase change enthalpy is represented by an apparent heat capacity, a raise of 500% is considered. Thermal conductivity is also varying with temperature, the maximum value is located in the same temperature range. These variations are shown in Fig. 3. The thermal contact resistances are put equal to zero—its values are not substantial in a simulated problem, while they are supposed known. Temperature histories $T_0(t)$ and $T_L(t)$, are shown in Fig. 4. They are similar to these recorded ordinarily in the apparatus. The discretisation parameters are chosen as follows: $N = 50$ (space discretisation), NT is calculated in order to have the Fourier number close to one, i.e.

$$\left(\lambda_{\max}\frac{t_f}{NT}\right)\Big/\left(C_{\min}\frac{L^2}{(N-2)^2}\right)\approx 1.$$

Thermal conductivity to be identified is described by an irregular grid of seven points ($\theta_j = 80$, 100, 120, 125, 130, 140 and 150°C) in the range of the temperature measurement. The iterative research is initialised with the parameter values $\beta_j^{(k=0)} = 0.4$, $j = 1, \ldots, 7$. The value of regulating coefficient δ, equation (17), is not critical, it can be taken between 1 and 100. Descent depth ε, equation (11(a)), is reduced to 0.7.

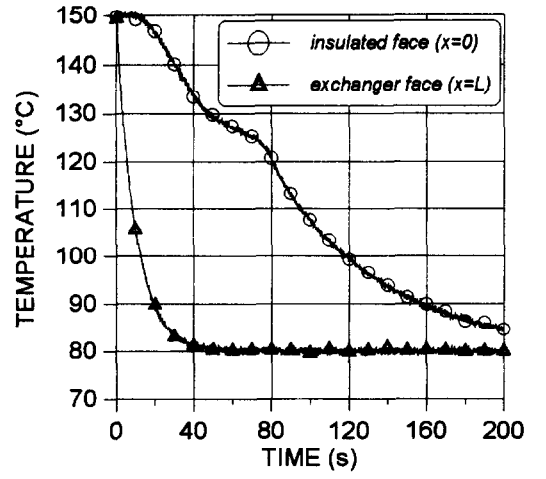

Fig. 4. Temperature histories on the sample's faces.

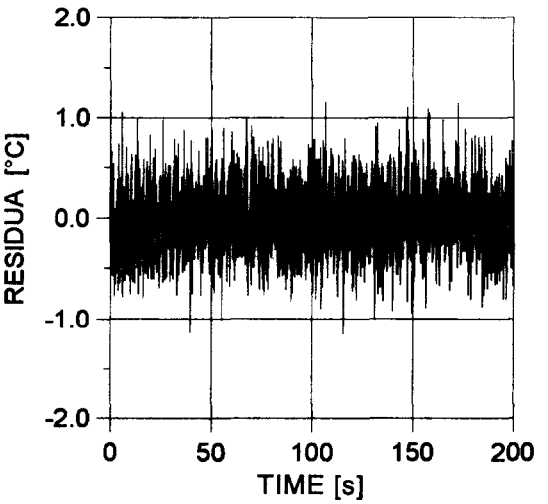

Fig. 5. Temperature residua obtained from noised data ($\sigma = 0.35$ K).

Both the exact and noised data were proceeded. In the first case, the parameters β^* which are finally estimated, correspond with five significant digits to the exact values β^{ex}. For highly noised temperature data ($\sigma = 0.35$ K, that is: $\sigma/\Delta T = 0.5\%$), identification error: $\sup[|\beta_j^* - \beta_j^{ex}|/\beta_j^{ex}]$ is less than 0.04. The Fig. 5 gives the residual $Y - \eta(\beta)$ obtained with these data. It can be observed that this residual has the same characteristics that the noise: zero mean and $\sigma = 0.35$ K. Moreover, it has been observed that stability and convergence of the iterative procedure are independent of measurement noise. In fact, for actual measurements, data noise on temperature is 10 times lower than in this numerical experiment. The number of iterations needed to reach the minimum of the criterion is less than 40.

Different tests have been carried out. Some results are presented in [17]. It has been observed that:

- the numerical solution of the direct problem equations should be obtained with good accuracy. For example, with the same discretisation steps, the pure implicit scheme is less accurate than the Crank–Nicolson one. Its numerical error on the model response can induce identification errors of several per cent,
- convergence difficulties in the iterative process are often related to strong nonlinearity of the model equations. High values of phase change enthalpy and short temperature interval would lead to instabilities,
- inaccurate data on the phase change temperature can cause a perturbation of the identified parameters values in this range.

Comparison with other methods

The same numerical data (i.e. exact and noised) are then processed with Gauss, Levenberg and Marquardt methods. The iterative processes leads to the following observations and comments:

- no convergence is observed with Gauss method;
- convergence with a Levenberg method is achieved toward the exact values, provided that appropriate values of the regulating coefficients are chosen, but convergence speed is extremely slow (more than 300 iterations are needed);
- convergence with a Marquardt method is obtained, but toward erroneous values (error is greater than 10%) and in the best cases twice as long as our method.

The similar conclusions concerning Levenberg and Marquardt methods, resulting from other tests were done by Davies and Whitting [7] and confirmed by Beck [14].

EXPERIMENTAL RESULTS

Description of the apparatus

The apparatus is shown in Figs. 6 and 7. It involves two main parts: the melting chamber and the mould. The mould is filled with melted material from a cylindrical melting chamber located above the mould. Two pistons are used for filling and to control the pressure. The mould is a symmetrical configuration which involves two moulding cavities separated by a metallic plate, an injection channel, a lateral insulating ring and an external heat exchanger on each side of the central plate. Moulding cavities are cylindrical (diameter = 0.06 m, thickness = 0.004 m).

Before filling, melting chamber and mould are heated up to the temperature of the injected thermoplastic. Electrical heating and air cooling of the moulding units are both controlled from the heat exchangers. Heating wires are located on its external faces, cooling is ensured by air flow through the internal spiral ducts of the exchangers. External insulating plates (thickness = 10 mm) reduce thermal inertia of the system and external metallic plates (thickness = 55 mm) give the rigidity to the apparatus.

Instrumentation and control

Two kinds of temperature measurements are performed on the apparatus: one is to control the melting chamber and mould temperature, the other gives the transient data $T_0(t)$ and $T_L(t)$ required for the parameter identification algorithm. Location of sensors are shown in Fig. 8(a) and (b). Inside the central plate, three long and narrow holes (diameter = 0.2 mm) are drilled by electroerosion and thermocouples are welded at the bottom. One of them gives $T_0(t)$, the two others are used to confirm the one-dimensional heat transfer assumption [16]. This wiring is robust compared to a surface instrumentation. To measure the temperature at the interface between the sample and the heat exchanger, three thermocouple wires are fixed under the exchanger surface in long holes (diameter = 0.6 mm). This location avoids accidentally pulling out the wires. Thermocouples are welded into narrow slots (length × depth × width = 3 × 0.3 × 0.6 mm) at the surface. One of them gives $T_L(t)$, the role of the others is as in the central plate.

A first experiment with a well-known material (plexiglass) validates the method, then experimental results obtained in moulding conditions, with two thermoplastic materials are presented. Thermal conductivity of an amorphous thermoplastic (ABS: acrylonitrile-butadienstyrene) and of a semicrystalline (polyamide 6/6 a218v30) are measured.

Plexiglass experiments

In the temperature range [20°C, 70°C] of this experiment, plexiglass is solid. So, a simplified apparatus has been used which avoids melting. It consists of the same symmetrical configuration used for melted thermoplastics with a central metallic plate, but moulding chambers are replaced by two identical solid samples. Thickness is equal to 11.5 mm for the samples and to 4 mm for the plate.

A density value ρ has been measured equal to 1182 kg m^{-3}. The heat capacity c_p, Fig. 9, was measured with a differential scanning calorimeter (Perkin Elmer DSC-7), and measurement error was estimated to $\pm 2\%$. Thermal contact resistance was taken equal to 10^{-4} m^2 K W^{-1}, i.e. the maximum value for polished surfaces.

Errors of model parameters were: $\pm 0.5\%$ for heat flux density between the central plate and sample, $\pm 0.5\%$ for sample thickness and $^{+0\%}_{-100\%}$ for TCR. All these error values were used to determine confidence intervals for the estimated thermal conductivity results according to the above procedure. A measurement noise was also taken into account. To evaluate its standard deviation, a measurement corresponding to a constant temperature was recorded. A gaussian distribution was found with a zero mean and $\sigma = 0.01$°C.

In Table 2, the results of thermal conductivity identification are shown. The length of confidence intervals calculated by considering only measurement noise, would be less than ± 0.0001 W m^{-1} K^{-1} (relative error less than 0.05%!), they would not correspond to the actual error. The thermal conductivity results are in a good agreement with another exper-

Table 2. Plexiglass thermal conductivity

Temperature (°C)	Conductivity (W m^{-1} K^{-1})
20	$0.2017^{+0.0053}_{-0.0061}$
45	$0.2067^{+0.0053}_{-0.0061}$
70	$0.2099^{+0.0054}_{-0.0061}$

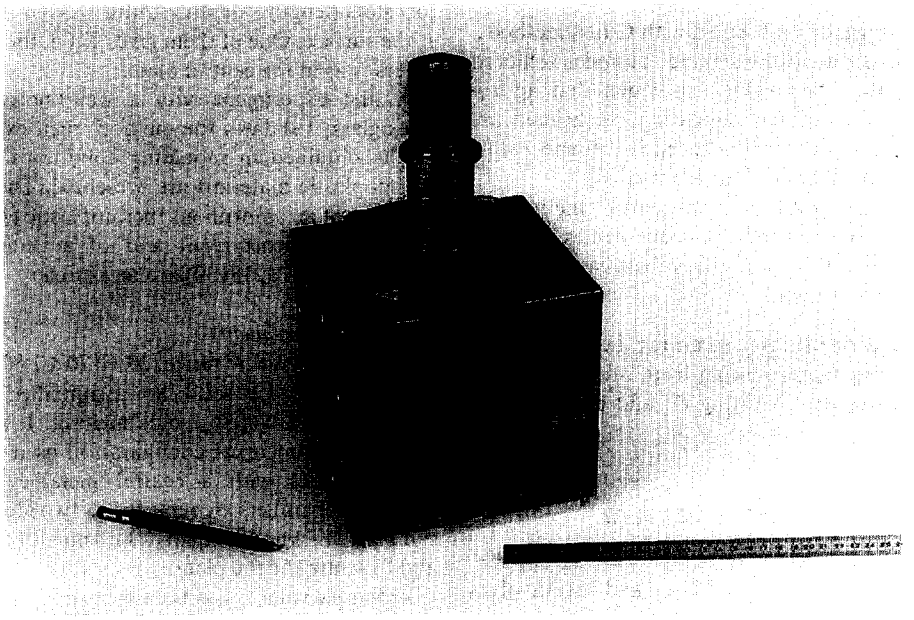

Fig. 6. Apparatus—main view.

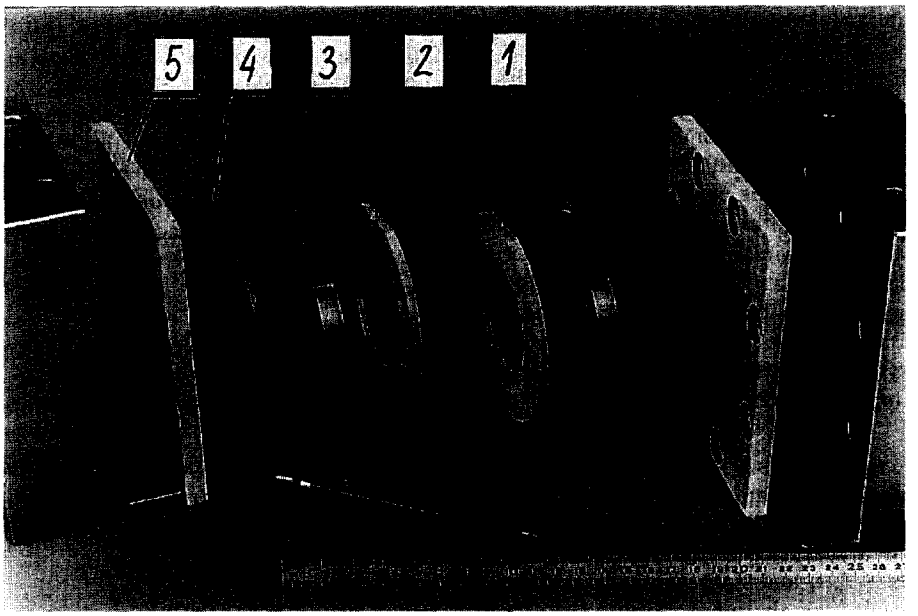

Fig. 7. Main parts of the conductivimeter: (1) central plate; (2) insulating ring; (3) heat exchanger; (4) plate for heating wires; (5) insulating plate.

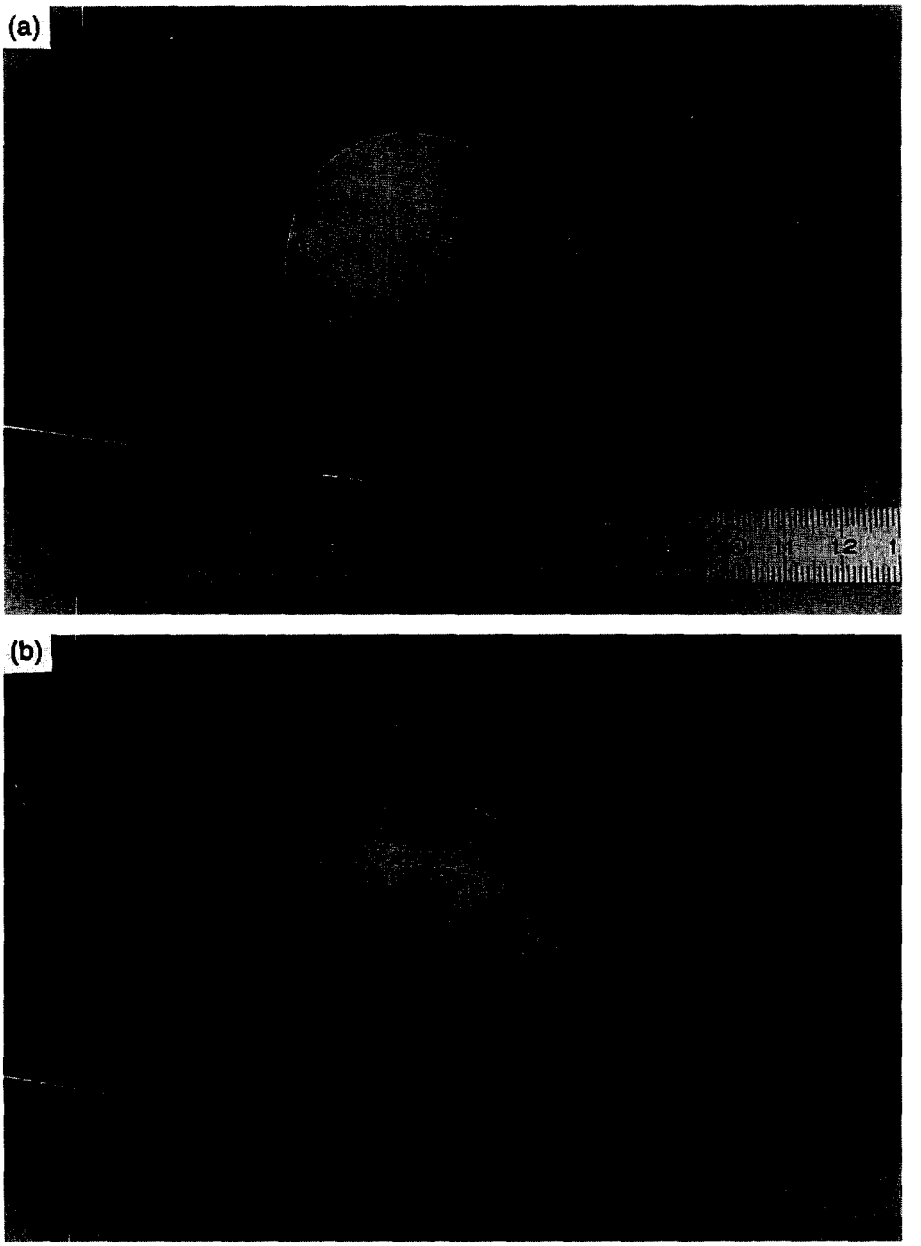

Fig. 8. (a) Sensor location—central plate. (b) Sensor location—heat exchanger.

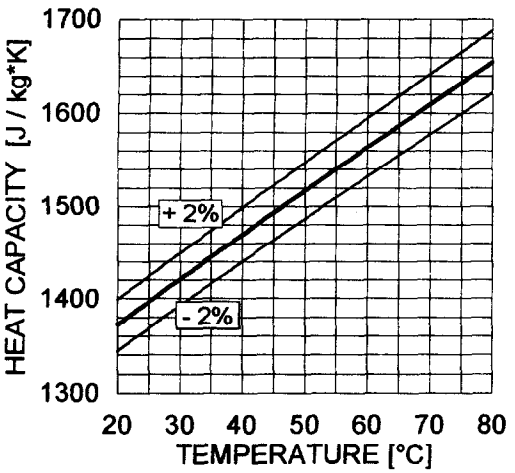

Fig. 9. Heat capacity of the plexiglass.

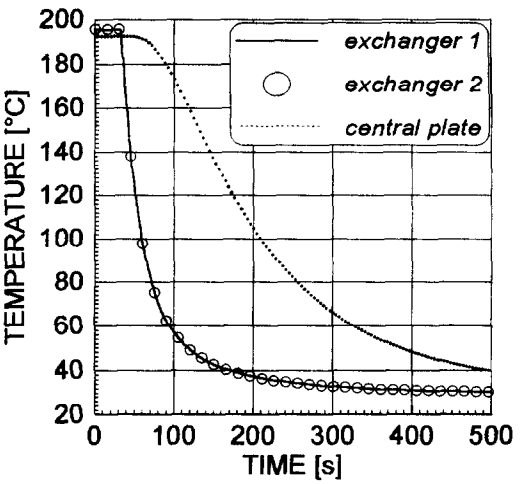

Fig. 11. Temperature records for the ABS.

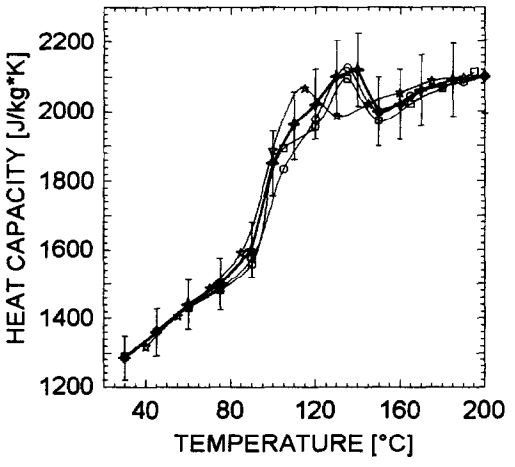

Fig. 10. ABS heat capacity (c_p).

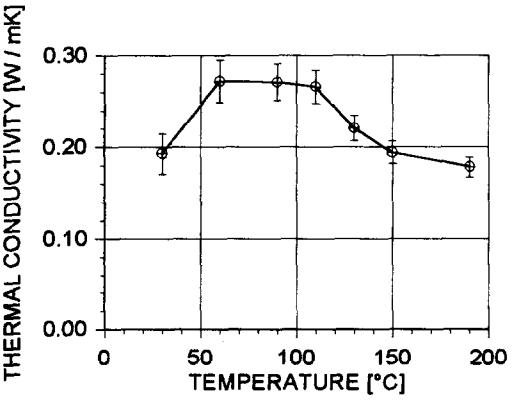

Fig. 12. Thermal conductivity of the ABS.

imental value, $\lambda = 0.21$ W m^{-1} K^{-1}, measured with a hot guarded plate method at $T = 35$°C.

Amorphous thermoplastic (ABS) experiments

The phase change enthalpy of this polymer is described by increasing heat capacity (c_p) in the corresponding temperature range. The DSC results obtained for different scanning velocities are difficult to reproduce. The c_p measurement accuracy is estimated to be $\pm 5\%$. Figure 10 shows the results obtained for two samples with different temperature rates and the average curve with the error intervals.

The polymer was injected in the moulding cavities at a temperature $T^0 = 200$°C, under a pressure of 40 MPa, pressure was held during the cooling period. The temperature histories of the exchangers and of the central plate during cooling, are presented in Fig. 11. TCR is supposed to be equal to zero when the sample is melted at the interface and to the maximum value (10^{-3} m^2 K W^{-1}) when it is solid. A linear variation is taken between these values during cooling.

Results of the ABS thermal conductivity are presented in Fig. 12.

To determine confidence intervals, errors on the model parameters are estimated to:

$\pm 5\%$ for volumetric heat capacity;
$\pm 5\%$ for heat flux density between central plate and sample;
$\pm 50\%$ for thermal contact resistance;
$\pm 0.5\%$ for sample thickness.

The resulting confidence intervals are in the range of 6–12%. It is important to underline that errors introduced in the model are not amplified by the identification method. Thermal conductivity obtained at ambient temperature (0.193 ± 0.022 W m^{-1} K^{-1}) is identical to that of the producer (0.19 W m^{-1} K^{-1}).

Semicrystalline thermoplastic experiments

A polyamide 6/6 a218v30, (30% of glass fiber) has been chosen. First, calorimetric measurements were performed in order to determine the crystallisation enthalpy, the heat capacity and phase change tem-

Table 3. Heat capacity of the polyamide 6/6 a218v30 (values out of the phase change zone)

Temperature [°C]	Heat capacity [J kg^{-1} K^{-1}]
50	1457
75	1658
100	1837
125	2016
150	2195
170	2171
190	2237
—	—
250	2266
270	2265
290	2092

perature of the material. The crystallisation enthalpy of a semicrystalline thermoplastic is several times greater than the enthalpy variation during solidification of an amorphous thermoplastic. This high value causes specific metrological difficulties to accurately determine and to measure its eventual variation with temperature. Another difficulty is in the determination of crystallisation temperature and its dependence on cooling rate. The following procedure has been used:

(1) Total enthalpy of crystallisation was measured first. Experiments were carried out with different cooling rates going from 5 to 50°C min^{-1}. We obtained 44513 J kg^{-1} ± 3%, with good reproducibility [15].

(2) The heat capacity out of the phase change interval was estimated. The c_p measurements are given in Table 3, error is less than ± 5%.

The accuracy for the apparent c_p values in the phase change range is not very good. Heat flux released by the sample and measured by the calorimeter during crystallisation, as a function of time and/or temperature, is strongly disturbed by several factors: thermal inertia of the apparatus, thermal inertia of the sample and thermal contact resistances. Furthermore, the temperature control of the samples, especially in this temperature range is not accurate. Device calibration is done for a constant cooling (or heating) rate and is no longer valid during phase change periods where large amounts of energy are liberated. Therefore, the crystallisation temperature and its eventual variation with cooling rate should be determined in a more accurate manner.

The determination of the solidification temperature is also difficult by usual DSC measurements. To investigate thermal behaviour of the material, a thermocouple was installed inside the sample during cooling. Experiments were done with different cooling rates. For each run the temperature history showed a plateau in the solidification interval. For this material, no dependence between the solidification temperature and cooling rate can be shown. Calorimetric measurements cannot give us accurate data for enthalpy variation. For the identification procedure, a regular variation (sinusoidal approximation) of the apparent heat capacity has been chosen, in the interval 215 ± 3°C.

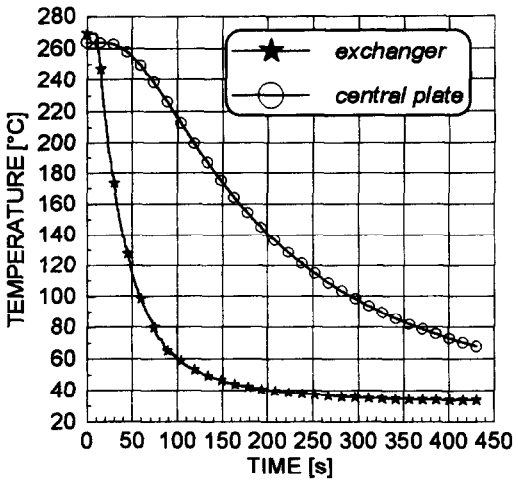

Fig. 13. Temperature histories for polyamide 6/6 a218v30.

The conditions for conductivity measurements were taken as follows: injection temperature equal to 270°C and pressure about 40 MPa, time of the experiment equal to 430 s. Figure 13 shows temperature histories on both sides of the sample. Table 4 gives the identified thermal conductivity values. To calculate the confidence intervals, errors on the model parameters were evaluated to: ± 5% for volumetric heat capacity, ± 5% for heat flux density, ± 50% for thermal contact resistance, ± 0.5% for sample thickness. Because of calorimetric measurement difficulties, conductivity identification results in the solidification range are discarded. Confidence intervals vary from 5.5 to 12%. These results are presented in Fig. 14. The thermal conductivity of another semicrystalline thermoplastic (Appryl) was measured and results compared with a hot guarded plate method. At ambient temperature, the values 0.284 ± 0.020 W m^{-1} K^{-1} and 0.286 W m^{-1} K^{-1} were found, respectively [15].

Table 4. Thermal conductivity of polyamide 6/6 a218v30

Temperature [°C]	Thermal conductivity [W m^{-1} K^{-1}]
50	0.173 ± 0.014
80	0.210 ± 0.022
90	0.221 ± 0.023
110	0.257 ± 0.030
130	0.279 ± 0.033
150	0.305 ± 0.036
170	0.316 ± 0.038
190	0.342 ± 0.038
200	0.348 ± 0.039
[results discarded]	
240	0.311 ± 0.024
250	0.328 ± 0.026
255	0.322 ± 0.025
260	0.330 ± 0.023
265	0.345 ± 0.019

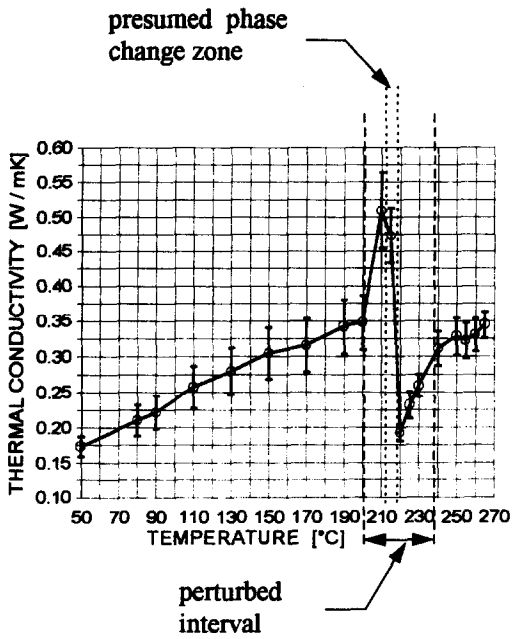

Fig. 14. Thermal conductivity for polyamide 6/6 a218v30.

CONCLUSIONS

An inverse method and a specific apparatus for the determination of polymer thermal conductivity have been described. Measurement of thermal conductivity is achieved for a large temperature domain with only one experiment, by cooling a sample of polymer from the melting phase to the solid phase. The pressure is fixed as in industrial moulding conditions. Thermocouples are installed only in the fixed parts of the apparatus, not in the polymer.

Classical conductivity measurement methods cannot ensure the required conditions of pressure and temperature. The method based on the resolution of an inverse heat conduction problem allows us to determine thermal properties during a phase change. Modelling equations could be more complex and involve a source term with a kinetic equation.

The iterative method consists in minimising a quadratic temperature residual criterion. The most efficient algorithm was searched for. Concerning accuracy and convergence speed, Gauss' method was found to be the best, for the slightly nonlinear problems. Methods which combine a descent direction of Gauss and a gradient direction were observed to be the slowest (Levenberg modified, Levenberg, Marquardt, Spiral). Moreover, the amount of computation for each iteration is at least twice as long, compared to Gauss' method. The method we developed is a modified Gauss method. To avoid singularity of the matrix X^TX and/or initial divergence of the iterative procedure, the diagonal of X^TX is appropriately changed at each iteration.

The evaluation of confidence intervals resulting from model parameter errors has been described. This error analysis has been also used to design the apparatus. Two main advantages follow from the multilayer symmetrical configuration: (1) accurate estimation of heat flux $\varphi_0(t)$ and temperature $T_0(t)$ at the same boundary of the sample is performed; and (2) no amplification of the model parameter errors on the estimated parameters is observed. Most the estimation errors come from enthalpy measurement error. Differential scanning calorimeter measurements to determine heat capacity variation for phase change materials are often not accurate enough and should be improved.

REFERENCES

1. Jarny, Y., Delaunay, D. and Bransier, J., Identification of non linear thermal properties by an output least square method. *Proceedings of the 8th International Heat Transfer Conference*, San Francisco, CA, 1986.
2. Jurkowski, T., Mise en oeuvre d'une méthode et réalisation d'un appareillage de mesure de la conductivité thermique d'un polymère. PhD thesis, Chap. 6, ECN–ISITEM, Nantes University, 1993.
3. Beck, J. V. and Arnold, K. J., *Parameter Estimation in Engineering and Science*. Wiley, New York, 1977.
4. Beck, J. V. and Arnold, K. J., *Parameter Estimation in Engineering and Science*, Chap. 7. John Wiley, New York, 1977.
5. Bard, Y., *Nonlinear Parameter Estimation*. Academic Press, Orlando, FL, 1974.
6. Levenberg, K., A method for the solution of certain nonlinear problems in least squares. *Quarterly of Applied Mathematics*, 1944, **2**, 164–168.
7. Davies, M. and Whitting, I. J., *A Modified Form of Levenberg's Correction. Numerical Methods for Non-Linear Optimisation*, eds F. A. Lootsma. Academic Press, London, 1972, pp. 191–201.
8. Marquardt, D., An algorithm for least squares estimation of nonlinear parameters. *Journal of the Society of Industrial and Applied Mathematics*, 1963, **11**(2), 431–441.
9. Morrison, D., Methods for nonlinear least square problems and convergence proofs, tracking programs and orbit determination. *Proceedings of the Jet Propulsion Laboratory Seminar*, 1960, pp. 1–9.
10. Jurkowski, T., Mise en oeuvre d'une méthode et réalisation d'un appareillage de mesure de la conductivité thermique d'un polymère. PhD thesis, Chap. 4.1. ECN–ISITEM, Nantes University, 1993.
11. Beck, J. V. and Arnold, K. J., *Parameter Estimation in Engineering and Science*, Chaps 2.3, 3.3 and 7.7. John Wiley, New York, 1977.
12. Stoër, J. and Burlish, R., *Introduction to Numerical Analysis*. Springer, New York, 1983.
13. Jurkowski, T., Mise en oeuvre d'une méthode et réalisation d'un appareillage de mesure de la conductivité thermique d'un polymère. PhD thesis, Chap. 4.2. ECN–ISITEM, Nantes University, 1993.
14. Beck, J. V. and Arnold, K. J., *Parameter Estimation in Engineering and Science*, Chap. 7.6.4. John Wiley, New York, 1977.
15. Sommier, A., Jurkowski, T., Delaunay, D. and Jarny, Y., Characterization of thermophysical parameters of thermoplastic materials. *Proceedings of the 14th European Conference on Thermophysical Properties*, INSA, Lyon, 16–19 September 1996, Villeurbanne, France.
16. Jurkowski, T., Mise en oeuvre d'une méthode et réalisation d'un appareillage de mesure de la conductivité thermique d'un polymère. PhD thesis, Chap. 8.2. ECN–ISITEM, Nantes University, 1993.
17. Jurkowski, T., Jarny, Y. and Delaunay, D., Thermal metrology and inverse techniques. Ecole de Printemps SFT-GUT, Estimation de la conductivité thermique de thermoplastiques. Un appareil de mesure et un algorithme inverse. Compte-rendu de l'Ecole de Printemps, Centre CNRS d'Aussois, 19–25 March 1995.

APPENDIX

Table A1. Elements of the matrix for the direct problem equation

	$G_{i,1}$	$G_{i,2}$	$G_{i,3}$	$H_{i,1}$	$H_{i,2}$	$H_{i,3}$	V_i
$i=0$	—	1	-1	—	0	0	$R_0^{n+1}\varphi_0^{n+1}$
$i=1$	0	$\lambda_{i+1/2}^{n+1}+\frac{3C(U_{i+1/4}^{n+1/2})}{32M}$	$-\lambda_{i+1/2}^{n+1}+\frac{C(U_{i+1/4}^{n+1/2})}{32M}$	0	$-\lambda_{i+1/2}^{n+1}+\frac{3C(U_{i+1/4}^{n+1/2})}{32M}$	$\lambda_{i+1/2}^{n+1}+\frac{C(U_{i+1/4}^{n+1/2})}{32M}$	$\frac{\Delta x}{2}(\varphi_0^{n+1}+\varphi_0^n)$
$i=2$	$-2\lambda_{i-1/2}^{n+1}$	$2\lambda_{i-1/2}^{n+1}+\lambda_{i+1/2}^{n+1}+\frac{21C(U_{i+1/8}^{n+1/2})}{32M}$	$-\lambda_{i+1/2}^{n+1}+\frac{3C(U_{i+1/8}^{n+1/2})}{32M}$	$2\lambda_{i-1/2}^{n}$	$-2\lambda_{i-1/2}^{n}-\lambda_{i+1/2}^{n}+\frac{21C(U_{i+1/8}^{n+1/2})}{32M}$	$\lambda_{i+1/2}^{n}+\frac{3C(U_{i+1/8}^{n+1/2})}{32M}$	0
$i=3$ to $i=N-2$	$-\lambda_{i-1/2}^{n+1}$	$\lambda_{i-1/2}^{n+1}+\lambda_{i+1/2}^{n+1}+\frac{C(U_i^{n+1/2})}{M}$	$-\lambda_{i+1/2}^{n+1}$	$\lambda_{i-1/2}^{n}$	$-\lambda_{i-1/2}^{n}-\lambda_{i+1/2}^{n}+\frac{C(U_i^{n+1/2})}{M}$	$\lambda_{i+1/2}^{n}$	0
$i=N-1$	$-\lambda_{i-1/2}^{n+1}+\frac{3C(U_{i-1/8}^{n+1/2})}{32M}$	$\lambda_{i-1/2}^{n+1}+2\lambda_{i+1/2}^{n+1}+\frac{21C(U_{i-1/8}^{n+1/2})}{32M}$	$-2\lambda_{i+1/2}^{n+1}+$	$\lambda_{i-1/2}^{n}+\frac{3C(U_{i-1/8}^{n+1/2})}{32M}$	$-\lambda_{i-1/2}^{n}-2\lambda_{i+1/2}^{n}+\frac{21C(U_{i-1/8}^{n+1/2})}{32M}$	$2\lambda_{i+1/2}^{n}$	0
$i=N$	$-W_1\lambda_{i-1/2}^{n+1}+W_2$	$W_1\lambda_{i-1/2}^{n+1}+3W_2+1$	0	$W_1\lambda_{i-1/2}^{n}+W_2$	$-W_1\lambda_{i-1/2}^{n}+3W_2-1$	0	$T_L^{n+1}+T_L^n$

$$M=\frac{\Delta t}{2(\Delta x)^2}\quad W_1=\frac{2R_L^{n+1/2}}{\Delta x}\quad W_2=\frac{\Delta x R_L^{n+1/2}C(U_{i-1/4}^{n+1/2})}{8\Delta t}\quad \Delta x=\frac{L}{N-2}$$

NB: The second index of the matrix [G] and [H] elements denotes the diagonal numbers.